Published in final edited form as:
*J Biol Chem*. 2008 January 11; 283(2): 875–888.

# Picornavirus genome replication: Identification of the surface of the poliovirus (PV) 3C dimer that interacts with PV 3Dpol during VPg uridylylation and construction of a structural model for the PV $3C_2$-3Dpol complex*

**Miaoqing Shen**[1,2], **Zachary J. Reitman**[1,3], **Yan Zhao**, **Ibrahim Moustafa**, **Qixin Wang**, **Jamie J. Arnold**, **Harsh B. Pathak**[4], and **Craig E. Cameron**
*From the Department of Biochemistry & Molecular Biology, The Pennsylvania State University, University Park, Pennsylvania, 16802*

## Abstract

Picornaviruses have a peptide termed VPg covalently linked to the 5′-end of the genome. Attachment of VPg to the genome occurs in at least two steps. First, Tyr-3 of VPg, or some precursor thereof, is used as a primer by the viral RNA-dependent RNA polymerase, 3Dpol, to produce VPg-pUpU. Second, VPg-pUpU is used as a primer to produce full-length genomic RNA. Production of VPg-pUpU is templated by a single adenylate residue located in the loop of an RNA stem-loop structure termed oriI by using a slide-back mechanism. Recruitment of 3Dpol to and its stability on oriI has been suggested to require an interaction between the back of the thumb subdomain of 3Dpol and an undefined region of the 3C domain of viral protein 3CD. We have performed surface-acidic-to-alanine-scanning mutagenesis of 3C to identify the surface of 3C with which 3Dpol interacts. This analysis identified numerous viable PV mutants with reduced growth kinetics that correlated to reduced kinetics of RNA synthesis that was attributable to a change in VPg-pUpU production. Importantly, these 3C derivatives were all capable of binding to oriI as well as wild-type 3C. Synthetic lethality was observed for these mutants when placed in the context of a PV mutant containing 3Dpol-R455A, a residue on the back of the thumb required for VPg uridylylation. These data were used to guide molecular docking of the structures for a poliovirus 3C dimer and 3Dpol, leading to a structural model for the $3C_2$-3Dpol complex that extrapolates well to all picornaviruses.

## INTRODUCTION

Picorna- and picorna-like viruses cause diseases in humans, animals, insects and plants (1,2). The genome of these viruses is a single-stranded RNA of positive polarity that is, on average, 7500 nucleotides (nt) in length that contains a protein, VPg (virion protein genome-linked) covalently attached to its 5′-end (1,2). Picornavirus negative-strand RNA also contains VPg covalently attached to its 5′-end (1,2). The role(s) of VPg in the metabolism of the viral genomic

*This work was supported, in part, by a research grant from NIH/NIAID AI053531 to C.E.C. C.E.C. is the recipient of an Established Investigator Award (0340028N) from the American Heart Association. Z.J.R. is the recipient of a Department of Homeland Security Scholarship.

Address correspondence to: Craig E. Cameron, Department of Biochemistry and Molecular Biology, Pennsylvania State University, 201 Althouse Laboratory, University Park, PA 16802, Tel.: 814-863-8705; Fax: 814-865-7927; E-mail: cec9@psu.edu.
[1]These authors contributed equally to this study.
[2]Current address: Department of Biomedical Sciences, Cornell University, Ithaca, NY 14853
[3]Current address: Medical Scientist Training Program, Duke University School of Medicine, Durham, NC 27705
[4]Current address: Department of Medical Oncology, Fox Chase Cancer Center, Philadelphia, PA 19111

and antigenomic RNA is not known but could prevent recognition by the innate immune system, enhance RNA stability and/or contribute to efficient packaging of the viral genome.

Attachment of VPg to the 5′-end of picornaviral RNAs is, minimally, a two-step process. Tyr-3 of VPg, or some precursor thereof, is used as a primer by the viral RNA-dependent RNA polymerase, 3Dpol, to produce VPg-pUpU, which, in turn, serves as a primer for production of full-length genomic and antigenomic RNAs (3). To date, two templates for 3Dpol-catalyzed uridylylation of VPg have been discovered: the poly(rA) tail located on the 3′-ends of all picornaviral genomic RNAs (4); an RNA stem-loop most often located in protein-coding sequence of picornaviral genomic RNA that has been termed the cre (cis-acting replication element) or oriI (origin of replication internal) (5,6). There is currently some debate regarding the use of one or both of these elements for VPg uridylylation. Some studies suggest that the poly(rA) tail is the template for production of VPg-pUpU employed for antigenomic RNA synthesis, and oriI is the template for production of VPg-pUpU employed for genomic RNA synthesis (7–9). Other studies suggest that oriI is the template for production of VPg-pUpU employed for both antigenomic and genomic RNA syntheses (10). In spite of this controversy, it is clear that oriI-templated production of VPg-pUpU is an essential reaction for picornavirus genome replication.

OriI-templated production of VPg-pUpU has been reconstituted in vitro from purified components for a variety of picornaviruses (5,10–14). Importantly, these in vitro systems explain and predict phenotypes observed biologically (5,10–14). The minimal requirements for efficient VPg uridylylation in vitro are: oriI, 3Dpol, VPg peptide, 3C(D) protein and UTP (5). OriI varies in length between picornaviruses, but all can be described as having a loop and a stem. The stem can be divided into two parts: upper-stem and lower-stem (3). The loop and upper-stem are both necessary and sufficient for efficient VPg uridylylation (3). Picornaviral 3CD protein is a fusion between 3C protease and 3D polymerase domains. Protein 3CD exhibits protease activity with a specificity and catalytic efficiency that is different than 3C but lacks polymerase activity, although the overall fold of the 3D domain of 3CD is quite similar to that of 3Dpol (15,16). In addition to protease activity, the 3C domain alone and in the context of 3CD exhibit both specific and non-specific RNA-binding activity (12,13,17–34).

Our current model for assembly and organization of the picornavirus VPg uridylylation complex is shown in Fig. 1. A dimer of 3C(D) binds to oriI with 3C domains interacting with the upper-stem of oriI (step 1) (13,14). This complex isomerizes to unwind the stem such that each of the 3C domains interacts with a strand of the stem in a sequence-specific fashion and the 3D domains interact with the lower-stem (step 2) (13,14). Information on the interaction between the 3D domain and the lower-stem is not currently available. Opening of the upper-stem of oriI by 3C(D) has been suggested to organize the loop into a conformation that should be readily accommodated by 3Dpol (13,35,36). 3Dpol is thought to be recruited to this complex and retained therein by an interaction between the back of the thumb subdomain of 3Dpol and an undefined surface of the 3C(D) dimer (step 3) (13,14). VPg or some precursor thereof joins the complex either along with (37,38) or after (39) 3Dpol. Finally, two rounds of UMP incorporation occur without dissociation of the peptide primer. Both uridylate residues are templated by a single adenylate residue by using a slide-back mechanism (40).

Molecular genetic, biological, biochemical and physical data support the existence of an interaction between 3Dpol and the 3C(D) dimer that is required for picornavirus VPg uridylylation (13,14,41). However, the specific surface(s) of 3C that interact with 3Dpol is unknown. We have used a reverse-genetic approach to identify residues of poliovirus (PV) 3C that interact with 3Dpol to facilitate formation and/or stabilization of the VPg uridylylation complex. We have identified numerous residues of 3C that localize to a single surface of the 3C dimer that influences VPg uridylylation efficiency in vitro and RNA replication and virus

production in cell culture. Importantly, only viable PV 3C mutants with slow-growth phenotypes attributable to VPg uridylylation defects unrelated to oriI-binding exhibited synthetic lethality with a PV 3Dpol mutant that is known to be impaired for VPg uridylylation in vitro (38). A structural model for the PV $3C_2$-3Dpol complex was constructed by using a docking algorithm that is consistent not only with all of the new data on 3C reported here but also with all of the data on 3Dpol published previously by us (13,14,41) and others (32,42, 43). This model extrapolates well to other members of the picornavirus family, thus providing a high-resolution perspective of the picornavirus VPg uridylylation complex. The impact of this model on our understanding of the structure, function, mechanism and evolution of picornavirus VPg uridylylation complexes and components thereof is discussed.

## EXPERIMENTAL PROCEDURES

### Materials

DNA oligonucleotides were from Integrated DNA Technologies, Inc.; Deep Vent DNA polymerase and restriction enzymes were from New England Biolabs, Inc.; Shrimp Alkaline Phosphatase was from USB; T4 DNA ligase was from Invitrogen; Difco-NZCYM was from BD Biosciences; QIAEX beads were from QIAGEN; RNase A was from Sigma; Ultrapure UTP solution was from GE Healthcare; [α-$^{32}$P] UTP (6000 Ci/mmol) was from Perkin-Elmer Life Sciences Inc.; Synthetic PV VPg peptide was purchased from Alpha Diagnostic International (San Antonio, Texas); HeLa S3 cells were obtained from American Type Culture Collection (ATCC) and grown in DMEM/F-12 medium with 10% fetal bovine serum (Invitrogen) with 100 U/mL penicillin and 100 U/mL streptomycin; 3′-fluorescein-labeled oriI (29 nt) was from Dharmacon, Inc.; All other reagents and apparatuses were available through Fisher, VWR or as indicated.

### Construction of Mutated Viral cDNA Clones and Replicons

A SacII site and HpaI site were introduced in the PV ORF of pMoRA at positions 4498 and 5207, respectively, by using overlap-extension PCR with the viral cDNA (pMoRA, also known as pXpA-rib+ polyAlong) and replicon (pRLucRA, also known as pRLuc-rib+ polyAlong) (44) as template. Two PCR fragments were amplified using oligonucleotides 1–4 (Table 1), and then these two fragments were used as templates for amplification of a new fragment using oligonucleotides 1 and 2 (Table 1). The PCR product with the HpaI site was cloned into the pMoRA plasmid using SnaBI and BglII sites to yield pMoRA-HpaI. Introduction of HpaI into pRLucRA was performed as described above except using SpeI and BglII sites (oligo 5 in Table 1). Oligonucleotides 6–9 (Table 1) were used to amplify fragments with a SacII site. The PCR product was cloned into pUC18-3CD-BglII-EcoRI (45) to yield pUC18-3CD-BglII-SacII-EcoR1 using BglII and AflII sites. The fragment with the SacII site in pUC18-3CD-BglII-SacII-EcoR1 was cloned into the pMoRA-HpaI and pRLuc-HpaI using BglII and EcoRI or BglII and ApaI, respectively, to yield pMoRA-HpaI-SacII and pRLuc-HpaI-SacII.

A subclone, pUC18-3A-3C-HpaI-SacII, was created to facilitate mutagenesis.. To create this plasmid, pUC18-3CD-BglII-EcoRI (45) was digested with PstI and EcoRI to remove the 3C–3D coding region. Oligonucleotides 40 and 41 (Table 1) were annealed to form a linker containing HpaI and SacII sites with PstI and EcoRI ends. This linker was ligated into the digested pUC18-3C-3D-BglII-EcoRI. The HpaI to SacII insert from pRLucRA, containing the 3B, 3C, and part of the 3A PV coding region, was cloned into the newly introduced restriction sites of this plasmid to form pUC18-3A-3C-HpaI-SacII.

The QuikChange® site-directed mutagenesis kit (Stratagene) was employed to introduce mutations into 3C-coding sequence with oligonucleotides 10–35 (Table 1) The resulting plasmids were used as templates for PCR with oligonucleotides 4 and 8 (Table 1). The PCR

product was inserted into the SacI and HpaII sites of pMoRA-HpaI-SacII and pRLucRA-HpaI-SacII to produce pMoRA-HapI-SacII-3C-Acidic-to-Alanine and pRLucRA-HpaI-SacII-3C-Acidic-to-Alanine, respectively.

Introduction of the R455A mutation into the 3D thumb subdomain in the viral cDNA required overlap extension PCR by using oligos 2, 37–39 (Table 1) and the viral cDNA, pMoRA, as the template. The PCR product was digested with MfeI and EcoRI and subcloned into the intermediate plasmid, pUC18-BglII-EcoRI-3CD (referred to as pUC-3CD in (45)). From this subclone, the fragment between ApaI and AvrII was cloned into pRLuc-HpaI-SacII to yield the thumb mutant replicon (pRLuc-HpaI-SacII-3D-R455A). To introduce the mutation into pMoRA-HpaI-SacII, the fragment between the ApaI and SacII sites from the pRLuc-HpaI-SacII-R455A plasmid was digested, gel purified and cloned into pMoRA-HpaI-SacII to yield pMoRA-HpaI-SacII-R455A. To introduce the R455A mutation into the pRLucRA-HapI-SacII-3C-Acidic-to-Alanine and pMoRA-HpaI-SacII-3C-Acidic-to-Alanine plasmids, the fragment between the ApaI and SacII sites from the pRLuc-HpaI-SacII-R455A plasmid was digested, gel purified and cloned.

## Subgenomic Replicon Assays

RNA replicon transcripts were prepared as previously described (41). RNA transcripts (5 μg) were electroporated into HeLa cells ($1.2 \times 10^6$ in 400 μL PBS) as previously described (41) and these electroporated cells were immediately transferred to 5.6 mL of pre-warmed (37 °C) media (DMEM/F12). 500 μL aliquots were prepared in microcentrifuge tubes and incubated on a rocker at 37 °C. At each time point (0, 2, 4, 6, 8 and 10 h), the cells were pelleted by centrifugation at 14,000 *x g* for 2 min, and 100 μL of cell culture lysis reagent (Promega) was added to the cell pellet. Lysates were left on ice at 4 °C until all time points were collected. Assays were performed by mixing 10 μL of lysate with 10 μL of luciferase assay substrate (Promega) and luciferase quantification was carried out as described by the supplier with a Junior LB 9509 luminometer (Berthold). Assays performed in the presence of 3 mM guanidine-HCl (GuHCl), a reversible inhibitor of PV RNA replication (46–48), were used as negative controls.

## In Vitro Translation Assays

RNA replicon transcripts were synthesized as described above. Translation reactions were carried out at 30 °C for 2 h in the presence of 1 μCi of [$^{35}$S]-methionine (Amersham Biosciences) with HeLa S10 translation mixtures as previously described (41,49,50). The mixtures contained 60% by volume S10, 10% by volume initiation factor (rabbit reticulocyte lysate, Promega), 10% by volume 10X nucleotide mix (10 mM ATP, 2.5 mM GTP, 2.5 mM UTP, 600 mM $KCH_3CO_2$, 300 mM creatine phosphate, 4 mg/mL creatine kinase, and 152 mM HEPES, pH 7.5), 2 mM guanidine-HCl and 4 μg/mL replicon RNA. After 2 h incubation at 30 °C, samples (5 μL) were mixed with 30 μL of SDS-PAGE sample buffer (2% SDS, 62.5 mM Tris-HCl (pH 6.8), 20% glycerol, 0.5% β-mercaptoethanol, and 0.1% bromophenol blue). The samples were heated at 90 °C for 5 min and samples (5 μL) were loaded on 12.5% SDS-polyacrylamide gels. Gels were fixed, dried and the radiolabeled proteins were detected by phosphorimaging.

## Virus Isolation, Virus Titer and One-step Growth Curves

Viral RNA transcripts were synthesized as previously described (41). HeLa cells ($1.2 \times 10^6$, 400 μL in PBS) were transfected with 5 μg viral RNA transcript as described above for the subgenomic replicon assays. Electroporated cells were immediately transferred to 400 μL of pre-warmed (37 °C) media (DMEM/F12) and added to HeLa cell monolayers (100 mM dishes) with 9.2 mL DMEM/F12 media. After incubation at 37 °C for 2 days, viruses were harvested by 3 repeated freeze-thaw cycles and used as stocks for analysis of plaque assays. The virus

was serially diluted in PBS ($10^{-2}$, $10^{-4}$, $10^{-5}$, $10^{-6}$ and $10^{-7}$) and 100 μL of each dilution was placed on cells ($6 \times 10^5$ cells each) in 6-well dishes. 200 μL of PBS was added to each well and the mixture was incubated for 20 min at room temperature to allow the virus to adsorb to the cells. PBS was replaced with 3 mL of 1X DMEM/F12 plus 10% fetal bovine serum and 1% agarose was added to each well. After 2 days of incubation, the agarose overlay was removed and the cells were stained with crystal violet. Plaques were counted to determine virus titer. To analyze one-step virus growth, cells in 6-well plates were infected with virus at a multiplicity of infection (MOI) of 10. After a 20 min incubation at room temperature to allow virus to adsorb, cells were washed with PBS to remove excess virus. The cells were incubated at 37 °C for 0, 1, 2, 3, 4, 6 and 8 h post-infection. Virus was harvested by 3 repeated freeze-thaw cycles and virus titers were performed by plaque assays for the given time point.

## Infectious Center Assays

Infectious center assays were performed as previously described (41). Briefly, HeLa cells were transfected with 5 μg of viral RNA transcript and these cells were serially diluted and plated onto HeLa cell monolayers. Four hundred μL of DMEM/F-12 was added to each well. Cells were allowed to adsorb to the plate for 1 h at 37 °C and then the medium/PBS was aspirated. Cells were covered with 3 mL of 1X DMEM/F12 plus 10% fetal bovine serum and 1% agarose. After 2 days of incubation, the agarose overlay was removed and the cells were stained with crystal violet.

## Construction of PV 3C Expression Plasmids

The expression vectors containing WT or mutated PV 3C sequence were made using overlap-extension PCR with pET26Ub-3C-C147G-CHIS (41) as template. First, two PCR fragments were amplified using oligonucleotides 8, 36 and 10–35 (Table 1), then the two fragments were used as templates for amplification of a new fragment using oligonucleotides 8 and 36 (Table 1). The fragment between SacII and EcoRI sites was cloned into pET26Ub-3C-C147G-CHIS plasmid to yield pET26Ub-3C-C147G-CHIS derivatives.

## Expression and Purification PV 3C Derivatives

E. coli BL21(DE3)pCG1 cells (51) were transformed with the pET26Ub-3C-C147G-CHIS derivative for protein expression. BL21(DE3)pCG1 cells containing the pET26Ub-3C-C147G-CHIS plasmid were grown in 100 mL of media (NZCYM) supplemented with kanamycin (25 μg/mL), chloramphenicol (20 μg/mL) and dextrose (0.4%) at 37 °C until an $OD_{600}$ of 0.8–1.0 was reached. Cells were then induced by adding isopropyl-β-D-thiogalactopyranoside (IPTG) (0.5 mM final) and grown at 25 °C for 4 h. Cells were harvested by centrifugation (6000 *x g*, 10 min), and the pellets were suspended in 4 mL of lysis buffer (100 mM potassium phosphate, pH 8.0, 20% glycerol, 10 mM β-mercaptoethanol, 500 mM NaCl, 2.8 μg/mL Pep A, 2.0 μg/mL leupeptin). The cell suspension was lysed by passing through a French press (SIM-AMINCO). After lysis, phenylmethylsulfonyl fluoride (PMSF) and nonidet P-40 (NP-40) were added to final concentrations of 2 mM and 0.1%, respectively. Lysates were clarified by centrifugation for 30 min at 75,000 *x g* at 4 °C. The supernatants were then loaded onto Ni-NTA Spin columns (Qiagen). The columns were washed twice with 600 μL buffer A (50 mM HEPES, pH 7.5, 0.1% NP-40, 20% glycerol, 10 mM β-mercaptoethanol) containing 500 mM NaCl and 50 mM imidazole. Proteins were eluted with 500 mM NaCl in buffer A containing 500 mM imidazole. The eluted pooled fractions were dialyzed against 1 L of dialysis buffer (buffer A with 150 mM NaCl) at 4 °C for 3 h. After dialysis, protein concentration was determined at 280 nm in 6 M guanidine HCl, pH 6.5 using the extinction coefficient 0.007680 $\mu M^{-1}cm^{-1}$. Protein samples were analyzed on a 15% SDS-PAGE, which was stained with SYPRO Ruby stain (Invitrogen). The stained gel was scanned using a Typhoon variable mode

imager (Amersham). This approach permitted concentration of 3C to be determined by using a reference protein, thus excluding contributions of contaminants to the absorbance at 280 nm.

### VPg Uridylylation Assays

VPg uridylylation assays were performed essentially as previously described (41). The reaction mixture contained 1 μM 3C (WT or mutant), 1 μM PV 61-nt oriI and 10 μM VPg in reaction buffer (50 mM HEPES, pH 7.5, 5 mM magnesium acetate, 10% glycerol, 10 mM β-mercaptoethanol, 0.04 μM [α-$^{32}$P] UTP (6,000Ci/mmol) and 10 μM unlabeled UTP. All reactions were adjusted to a final concentration of 20 mM NaCl. Reaction mixture was preheated at 30 °C for 5 min. Reactions were initiated by addition of PV 3Dpol to 1 μM. All enzymes were diluted immediately prior to use in enzyme dilution buffer (50 mM HEPES, pH 7.5, 10 mM β-mercaptoethanol and 20% glycerol). After incubation at 30 °C for 30 min, the reaction was stopped by the addition of an equal volume (5 μL) of gel loading buffer (100 mM EDTA, 75% formamide, 0.025% bromophenol blue and 0.025% xylene cyanol). The quenched samples (5 μL) were analyzed by Tris-Tricine SDS-polyacrylamide gel electrophoresis. Gels contained 15% acrylamide and 0.4% bisacrylamide. The cathode buffer (upper chamber) contained 0.1 M Tris, 0.1 M Tricine, and 0.1% (w/v) SDS; the anode buffer contained 0.2 M Tris-HCl, pH 8.9. Gels were run at 80 watts (for a 33 – 39-cm gel) for 2.5 h. The incorporation of [α-$^{32}$P] UMP was visualized by using a PhosphorImager and quantified by using ImageQuant software.

### Fluorescence Polarization Assays

Experiments were performed using a Beacon fluorescence polarization system (GE Healthcare) as previously described (13). Assays were performed by mixing various concentrations of PV 3C (WT or mutant) with 0.1 nM 3′-fluorescein-labeled PV oriI (29-nt) in binding buffer (1 mM HEPES, pH 7.5 and 20 mM NaCl). Protein-RNA complexes were incubated for 30 s at 25 °C. Binding of PV 3C was measured by the change in polarization (Δ mP).

### Construction of the Molecular Model for the $3C_2$-3Dpol Complex

The atomic coordinates for PV 3C (1L1N) and PV 3Dpol (1RDR; partial structure missing the flexible fingers subdomain) were used as input files submitted to the GRAMM server (http://vakser.bioinformatics.ku.edu/resources/gramm/grammx/) to do the docking. The program GRAMM performs an exhaustive six-dimensional search through the relative translations and rotations of the molecules. The 3C molecule worked as the template and 3Dpol as the ligand in the docking run. Outputs for the top ten solutions from the server were investigated carefully using graphics. The model that was most consistent with the available molecular genetic and biochemical data was chosen for further refinement. The 3C dimer was placed in complex with the full structure of 3Dpol (1RA6; which possesses the fingers subdomain missing from the 1RDR coordinates). The 1RA6 structure was superimposed on top of the docked 3Dpol by using the program O (52). Residues in 1RA6 that had been mutated to produce crystals were returned to the wild-type amino acids by using the program O. To alleviate the apparent clashes between the 3C and the parts of the 3Dpol structure not included in the original docking, the model was further subjected to energy minimization using the CHARMM force field in the NAMD package (53). The input files for the energy minimization were prepared using the VMD program (54). The minimization stopped after 10,000 steps using the conjugate gradient minimizer; the relaxed structure was checked for unreasonable interactions by visual inspection and used as the final model.

# RESULTS

## Rationale

The first crystal structure of the RNA-dependent RNA polymerase (RdRp) from poliovirus (PV), 3Dpol, revealed extensive interactions between the back of the thumb subdomain of one 3Dpol molecule and the back of the palm subdomain of a second molecule that lead to formation of fibers of 3Dpol in the crystal (55). Since this time, numerous studies have been designed to prove a function for 3Dpol fibers (56–58). Interestingly, PV mutants containing changes in 3Dpol-coding sequence designed to prevent fiber formation exhibit different biological phenotypes in cell culture (41). For example, changes to the back of the thumb subdomain of 3Dpol are lethal to virus production due to a severe RNA synthesis defect (41,42); however, comparable changes to the back of the palm subdomain produce viable virus (41). Specifically, a PV mutant encoding a 3Dpol enzyme in which both Arg-455 and Arg-456, two residues on the back of the thumb of 3Dpol, are mutated to Ala (3Dpol-R455,456A) is inviable (42). In the context of a subgenomic replicon, these amino acid substitutions prevent RNA synthesis (41). Studies of 3Dpol-R455,456A and related derivatives in vitro show the inability of these enzymes to form fibers in vitro without any change in the RdRp activity on RNA-primed templates (41). However, these derivatives are incapable of being stimulated by 3C(D) in oriI-templated VPg uridylylation experiments (41). This observation provided the first hint that a physical interaction between the back of the thumb of 3Dpol and 3C(D) exists that functions during VPg uridylylation (41). Subsequent studies provided additional functional and physical evidence for the existence of this interaction (13).

Because at least one Arg residue of 3Dpol participated in the interaction with 3C (41) and this interaction appeared to be quite sensitive to the concentration of salt employed (38), we hypothesized that at least one acidic amino acid residue of 3C participated in the interaction with 3Dpol. If this hypothesis is correct, then by changing this residue to Ala, a PV mutant would be created that should exhibit a phenotype comparable to 3Dpol-R455,R456A PV mutant described above. Of course, any 3Dpol-interacting residue of 3C would be expected to reside on the surface of the protein. As shown in Fig. 2, 16 acidic amino acids exist on the surface of 3C. Proposed functions exist for many of these residues based on proximity to residues known to be involved in the RNA binding or protease activity of the protein (Table 2). In addition, some of these residues are located at the interface of the 3C dimer observed crystallographically, thus implying function (Table 2) (59). However, six of these residues do not have any known function (Table 2). Therefore, a surface-acidic-to-alanine mutagenesis approach had the potential not only to identify the surface of 3C that interacts with 3Dpol but also to test experimentally the proposed functions of several other surfaces of 3C.

## Study Design

All surface acidic amino acid residues of 3C were changed individually (single in Table 2) or in combination (double in Table 2) by site-directed mutagenesis of a shuttle vector containing 3C-coding sequence that permitted rapid sub-cloning of mutated DNA fragments into plasmids containing a PV genomic cDNA, a PV subgenomic replicon cDNA, or PV 3C-coding sequence under the control of a T7 RNA polymerase promoter. These constructs permit production of infectious virus in HeLa cells, evaluation of RNA synthesis in HeLa cells, or expression of 3C protein in Escherichia coli, respectively.

PV 3C(D) has two well-established functions during the PV lifecycle. 3C(D) is a protease responsible for cleavage of the viral polyprotein (1,2,15). 3C(D) is an RNA-binding protein that recognizes, in addition to oriI, replication elements at the 5′- and 3′-ends of the genome (17,19–21,23,27,31). However, functions for 3C(D) before and after RNA synthesis are also beginning to emerge (60–65). Because we were interested in identifying all phenotypes

associated with these mutants, a comprehensive analysis of the mutants was performed as described under Experimental Procedures. The specific infectivity of PV genomic RNAs encoding the various 3C mutants was determined by infectious center assay. Kinetics of virus production under one-step-growth conditions was determined for those alleles exhibiting a wt phenotype by infectious center assay. RNA synthesis was measured indirectly for all mutants by using the subgenomic replicon expressing luciferase. Proteolytic processing was evaluated by monitoring processing of the viral polyprotein produced by in vitro translation of subgenomic replicon RNA in a HeLa cell-free extract. Purified 3C proteins were evaluated for RNA binding and VPg uridylylation activities. Mutants of most interest to us here are those with growth defects due to defects in RNA synthesis unrelated to defects in proteolytic processing or RNA binding and exhibiting defects to VPg uridylylation in vitro.

### Specific Infectivity by Infectious Center Assay

PV genomic RNAs encoding each of the 13 3C mutants were prepared by in vitro transcription of mutated PV genomic cDNAs. RNAs were transfected into HeLa cells by electroporation. Transfected cells were diluted, plated onto a monolayer of HeLa cells, covered with an agarose overlay and incubated for two to three days at 37 °C. Monolayers were stained with crystal violet to visualize plaques. Specific infectivity (plaques formed per microgram of RNA) was calculated and reported as values relative to wt RNA (Table 3). Three phenotypes were observed. The specific infectivity of eight of the mutated RNAs (D5A, D32A, E45A, D50A, E53A/E55A, D58A/E63A, E81A and E121A) was equivalent to wt RNA. The specific infectivity of two of the mutated RNAs (E24A, E96A/D99A) was reduced by 100 fold relative to wt RNA. Infectious virus could not be recovered from three of the mutated RNAs (D64A, E71A, D85A).

### Kinetics of Virus Growth

The kinetics of virus growth were evaluated for PV mutants whose specific infectivity was equivalent to wt PV. All of these mutants exhibited a reduced rate of virus growth; a representative set of data is presented in Fig. 3. The titer of each mutant at 6 h post-infection was compared to that for wt PV, revealing a 2- to 50-fold reduction in the rate of virus growth for these mutants (Table 3).

### Kinetics of RNA Synthesis

Because 3C protein and 3C-containing precursor proteins play roles in the virus lifecycle before, during and after RNA synthesis, it was important to identify those 3C mutants whose growth phenotypes were attributable to RNA synthesis. For these experiments, a subgenomic replicon encoding luciferase instead of the viral capsid proteins was employed. This replicon permits the kinetics of RNA synthesis to be monitored indirectly by measuring the specific activity of luciferase as a function of time. Luciferase specific activity is expressed as relative light units (RLU) observed per microgram of total protein. Transfected, replicon RNA can be translated to produce luciferase in the absence of replication. The signal that derives from translation of the transfected, replicon RNA can be obtained by transfection of the replicon RNA into cells in the presence of 3 mM guanidine hydrochloride (GuHCl), an inhibitor of PV RNA synthesis (46–48).

All of the 3C mutants were evaluated in the context of the subgenomic replicon. Replicon RNAs were transfected into HeLa cells. At four and eight hours post-transfection, cell extracts were prepared and luciferase activity was measured. These two time points were chosen because they represent times in which replication is 50% or 100% complete for the wt replicon (Fig. 4). All of the mutated replicon RNAs exhibited a delay in the kinetics of RNA synthesis relative to wt replicon RNA (Fig. 4 and Table 3). As observed for the specific infectivity experiment, the mutants could be divided into three categories. Those mutants that failed to

produce virus also failed to replicate; these are: D64A, E71A and D85A. The D64A allele produced as much luciferase as wt replicon in the presence of GuHCl, suggesting that the stability and translatability of this RNA was normal. In contrast, the E71A and D85A alleles produced lower levels of luciferase at both time points evaluated, suggesting that stability and/or translatability of these RNAs may have been affected. One class of mutants exhibited a lower-than-expected reduction in replication efficiency relative to the observed kinetics of virus growth or specific infectivity. These are: D5A, E24A, E53A/E55A, D58A/E63A and E81A, E96A/D99A. These mutants may be defective in a post-replicative function of 3C or some precursor thereof in addition to having a function in replication. The final class of mutants exhibited reductions in RNA replication efficiency on par with that observed for the kinetics of virus growth. These are: D32A, E45A, D50A and E121A. These residues are likely only important for replication functions of 3C and/or its precursors.

## Proteolytic Activity of 3C Mutants

In order to determine if any of the growth and/or replication phenotypes were caused by inactivating 3C-dependent proteolysis, we performed in vitro translation experiments with subgenomic RNAs. Translation-competent HeLa extracts containing $^{35}$S-Met were programmed with each of the mutated replicon RNAs. Labeled products were resolved by SDS-PAGE and visualized by phosphorimaging (Fig. 5). Luciferase is produced co-translationally by the virus-encoded 2A protease and serves as control for RNA stability and gel loading. The other P2 and P3 proteins are processed by 3C-dependent activities. With the exception of the E71A and D85A mutants, all other mutants exhibited wt levels of processing. Identical effects have been observed for other substitutions at these positions of 3C (66). Unfortunately, this experiment is not sensitive enough to reveal subtle differences in kinetics of proteolysis.

## VPg Uridylylation

In order to identify 3C mutants with replication defects that could be attributable to VPg uridylylation, we expressed each of the 3C mutants in E. coli. With the exception of D85A protein, all other proteins were soluble. All 3C proteins contained a carboxy-terminal, hexa-histidine tag. Soluble proteins were purified to greater than 80% purity in a single step by using a nickel nitrilotriacetic acid agarose spin column. A representative set of purified proteins is shown in Fig. 6A.

PV VPg uridylylation—that is, production of VPg-pUpU and VPg-pU, can be recapitulated in vitro from purified components: 3Dpol, 3C, oriI, VPg and [α-$^{32}$P] UTP. The ability of each protein to function in this reaction was measured. A representative experiment is shown in Fig. 6B. The uridylylation efficiency for all soluble 3C derivatives was determined in at least three different experiments. The average uridylylation efficiency for each derivative is shown in Table 3. Four of the 3C derivatives exhibited at least a 2-fold reduction in VPg uridylylation. These are: D5A, E45A, E71A and E96A/D99A. Two of the 3C derivatives: E24A and D50A exhibited an increase in VPg uridylylation on the order of 2-fold greater than wt 3C. The remaining 3C derivatives did not exhibit a substantial difference (2 fold or greater) in VPg uridylylation activity relative to wt 3C.

## OriI Binding

The last experiment that we performed to screen the mutants was an RNA-binding experiment. 3C protein has two roles in VPg uridylylation: binding to oriI and recruitment of 3Dpol (13, 14). Changes in VPg uridylylation could be caused by changes in either activity. We used a fluorescence polarization assay to characterize binding of 3C derivatives to oriI (13). As shown in Fig. 7A, WT 3C was titrated into binding reactions containing fluorescein-labeled oriI under the same buffer conditions employed for VPg uridylylation. The change in fluorescence

anisotropy (Δ mP) was plotted as a function of 3C concentration. The data were fit to a hyperbolic binding equation by using a non-linear regression algorithm, yielding an equilibrium dissociation constant ($K_d$) value of 260 ± 40 nM. Each of the 3C derivatives was evaluated at a single protein concentration, 150 nM, which is in the linear range of the hyperbola. The observed fluorescence anisotropy was measured and compared to wt 3C (Fig. 7B and Table 3). Of the six 3C derivatives that exhibited changes in VPg uridylylation, only one of these (D5A) exhibited a reduction in oriI-binding activity. Crosslinking experiments failed to report a change in 3C dimerization, which could also cause changes in oriI binding or 3Dpol recruitment (data not shown).

## The Surface of 3C Dimer Required for VPg Uridylylation Interacts with 3Dpol

Thus far this study has defined five residues that fit the criteria for 3Dpol-interacting residues: E24, E45, E71, D96 and D99. Most appear on a single convex surface of the 3C dimer. We reasoned that if this is the surface that interacts with 3Dpol, then 3C mutants with changes on this surface might exhibit synthetic lethality in the context of 3Dpol-R455A, a mutant with a slow replication phenotype due to a defect in VPg uridylylation (38). The conceptual framework for this experiment is shown in Fig. 8A. Essentially, combining residues that contribute to the same function, stabilizing the same interface in this case, would be more deleterious than combining residues with different functions. For this experiment, three different 3C mutants were selected: E45A, E96A/D99A and E53A/E55A. All three of these mutants exhibit equivalent reductions in virus growth and replication; however, only the first two are thought to contribute to an interaction with 3Dpol that is required for VPg uridylylation (Table 3). All three mutants replicate equivalently in a background that contains WT 3Dpol (Fig. 8B). In contrast, E45A and E96A/D99A are lethal to replication in the 3Dpol-R455A background (Fig. 8B). Importantly, E53A/E55A did not cause any additional defect to replication of the 3Dpol-R455A mutant (Fig. 8B). We conclude that these and related residues of 3C-containing precursors contribute to a surface employed for recruitment and retention of 3Dpol to the VPg uridylylation complex.

## Structural Model for the $3C_2$-3Dpol Complex

High resolution crystal structures for the PV 3C dimer and PV 3Dpol are available (59,67). Having implicated a surface of the 3C dimer that interacts with 3Dpol, coupled with our previous studies that identified residues of 3Dpol essential for the interaction with the 3C dimer (13,14), we were confident that we had sufficient information to begin to distinguish between mutually exclusive solutions of complexes identified by using computational approaches. We have employed a well-established molecular docking algorithm (68) to obtain a structural model for the $3C_2$-3Dpol complex. Ten solutions were returned. One solution was completely consistent with all of our molecular genetic and biochemical data (13,14,41).

The model is shown in Fig. 9. Both the thumb and fingers subdomains of 3Dpol interact with the “top” of the 3C dimer, the side containing the protease active sites. The complex buries 1987 $Å^2$ of the solvent accessible surface area. The complex has a non-planar, interwoven interface with a high degree of complementarity between the surfaces of the 3C dimer and 3Dpol. Both side chain and backbone atoms contribute interactions to the interface. A channel is formed at the interface of the proteins (Fig. 9B). The channel is approximately 10Å in diameter and 36 Å in length. These dimensions are consistent with accommodation of a single-stranded RNA molecule that is 10-nt long.

The thumb of 3Dpol contributes most of the interactions to the interface, at least 12 amino acid residues (Fig. 9D). Worth noting is the presence of residues 406 and 455; these are known to be essential for VPg uridylylation (14,32,38,41). In addition, residue 461, the carboxy-terminal residue is located at the interface. A PV 3Dpol derivative that contains a GSSG-$H_6$ extension

at the carboxyl terminus is as active as unmodified 3Dpol in RNA-primed synthesis (51) but completely lacks any VPg uridylylation activity (69). Only two residues of the fingers subdomain, K133 and Q134, contribute directly to the interface.

The residues of 3C dimer at the interface are clustered in three patches (Fig. 9E). One patch is on subunit A of 3C and interacts with residues of the fingers subdomain of 3Dpol. The other two patches reside on both subunits A and B of 3C and interact with the thumb subdomain of 3Dpol. A complete list of the interactions is provided in Table 4.

## DISCUSSION

The 5′-end of both plus- and minus-strand RNAs of all picornaviruses is linked to a protein, VPg, which is also referred to as 3B (1,2). Linkage of VPg to picornaviral RNAs requires uridylylation of VPg to form VPg-pUpU. This product then serves as primer for production of full-length plus- and minus-strand RNAs. All picornaviruses have a cis-acting replication element that we refer to as oriI that serves as an efficient template for VPg uridylylation (3). The oriI-templated VPg uridylylation reaction has been reconstituted in vitro from purified components for a variety of picornaviruses (5,10–14). As a result, there is clear consensus on the virus-encoded protein factors that are required for this reaction. In a minimal system, in addition to the viral RNA-dependent RNA polymerase, 3Dpol, the RNA-binding activity of 3C or some precursor thereof, for example 3CD, is required for efficient VPg uridylylation. The precise function for 3C(D) in VPg uridylylation is not known. As indicated in Fig. 1, we have recently proposed that a 3C(D) dimer binds to oriI, extending the loop for binding to the RNA-binding site of 3Dpol (13). Recruitment of 3Dpol to this complex and stability therein would be mediated by an interaction between the back of the thumb sub-domain of 3Dpol and an undefined sub-domain of 3C (13,14). The goal of this study was to identify the 3Dpol-recruitment/retention sub-domain of 3C. Again, this subdomain of 3C would likely function in the context of a precursor, for example 3CD.

Because arginine residues on the back of the thumb of 3Dpol were known to be required for recruitment to and/or retention in the VPg uridylylation complex (13,14,41), acidic residues on 3C seemed reasonable candidates for interaction with 3Dpol. Importantly, 16 solvent-accessible, acidic residues of 3C existed (Fig. 2). Many of these residues have either only implied function, for example intermolecular interactions based on structural information, or no known function (Table 2). We constructed a panel of PV mutants that encoded changes in 3C in which surface-acidic residues were converted to alanine (Table 2). The biological and biochemical activities of the 3C derivatives were evaluated (Figs. 3–7). These data are summarized in Table 3. None of the mutants exhibited a wild-type phenotype in all assays (Table 3). Four classes of mutants were identified and are discussed below. Importantly, one of these classes exhibited all of the properties consistent with a surface of 3C involved in recruitment of 3Dpol to the VPg uridylylation complex.

### Folding, Proteolysis and RNA-binding Functions

The first class of mutants encoded changes at positions of 3C with established functions or at positions whose functions were not mechanistically insightful. E85 appears to be important for folding of 3C and formation of the protease active site as this derivative produced an insoluble protein in E. coli (Table 3) and was unable to process the viral polyprotein in HeLa cells (Fig. 5). E71 is a well-known component of the catalytic triad of the protease active site of 3C (59,70), so it was not surprising that virus could not be recovered from the E71A mutant due to the proteolysis defect. However, as discussed below, unexpected roles for E71 in VPg uridylylation exist.

D32 has been shown to be required for in vitro assembly of the ribonucleoprotein (RNP) complex that contains the cis-acting replication element at the 5′-end of the poliovirus (PV) genome (oriL) (17). That study did not report any biological analysis of this particular 3C derivative (17). Our data suggest that the oriI-binding activity of 3C-D32A was equal to that observed for wt 3C (Table 3), and less than a 2-fold decrease was observed on replication of a subgenomic replicon RNA encoding this 3C derivative (Fig. 4). This apparent paradox can be interpreted in several ways. It is possible that precursor rather than processed forms of the proteins are employed for binding to these RNA elements in vivo, contributing independently to the RNA-binding activity of 3C-containing precursors and suppressing RNA binding defects in 3C observed in vitro. It is also possible that D32 is involved in a protein-protein interaction with other proteins in the RNP complex. Loss of this interaction may preclude observation of the complex by using a gel-mobility-shift assay but only have a minor effect in cells for the reasons discussed above. Regardless of the explanation for the observed difference, this result clearly illustrates why a complete range of assays is required to achieve a clear understanding of picornaviral protein functions.

The amino terminus of 3C has been implicated in RNA binding (20,35). 3C-D5A exhibited a 2-fold reduction in oriI binding that was sufficient to explain the 2-fold reduction in VPg uridylylation as well as the 3-fold reduction in genome replication (Table 3). However, none of these phenotypes were sufficient to explain the 50-fold reduction in virus production, suggesting another function. In contrast, residues in the vicinity of E121 have not been implicated in RNA binding. However, 3C-E121A exhibited a 20–30% reduction in oriI binding, causing a comparable reduction in VPg uridylylation and genome replication. These are the first PV mutants that exhibited a quantitative correspondence between VPg uridylylation activity in vitro and genome replication in cells. We have recently argued that PV produces far more VPg-pUpU than required for genome replication, thus preventing VPg uridylylation from affecting the kinetics of genome replication (14). This assertion may still be correct; the genome-replication phenotype associated with the D5A and E121A mutants may be a reflection of defects associated not only with oriI binding but also oriL and oriR binding.

## Post-replication Functions

The second class of mutants exhibited defects in virus production that were more severe (greater than 5 fold) than defects associated with RNA synthesis (Table 3), suggesting that 3C(D) or precursors thereof function not only during replication but also after replication. These mutants were: D5A, E53A/E55A, D58A/E63A and E81A. The D64A mutant was dead and could not be studied, but it is likely that this mutant belongs to this group given its close proximity to several members of this class. By using a cell-free system for PV synthesis, Paul and colleagues have shown that addition of 3C(D) to these extracts stimulates a post-replication step in PV synthesis by greater than 100 fold (64,65). Currently, it is thought that 3CD stimulates maturation of the PV virion (64,65). Similarly, it is possible that these amino acid substitutions alter the kinetics and/or specificity of capsid precursor processing, leading to problems with virion assembly and/or maturation. Although the mechanistic basis for this defect is not at all clear, these mutants should permit both genetic and biochemical approaches to be applied to this problem.

It is important to highlight the fact that this class of mutants failed to exhibit a phenotype by using an infectious center assay. There is no doubt that the infectious center assay is qualitative and really only measures viral RNA induced cell death, not virus assembly or spread. However, such striking differences between the outcome of the infectious center assay and virus infectivity have never been reported, most likely because both assays are not generally employed in the same study. The reason for this difference in not clear. Our data show that a

10-fold reduction in the kinetics of virus assembly and/or spread is not detected by this assay. We speculate that as long as translation and genome replication of the genome is fast relative to the two-day assay, even a cell infected with a reduced quantity of virus will die quite rapidly given the cytotoxicity of the viral proteins, especially the 3C and 3CD proteins.

### Pre-replication Functions

The third class of mutants exhibited specific infectivity defects that were more severe (10 fold) than RNA synthesis. These mutants were: E24A and E96A/E99A (Table 3). Given the discussion of the infectious center assay above, these mutants should be defective in translation or replication (directly or indirectly). Translation and processing appeared normal, at least in a cell-free extract (Fig. 5). The RNA-binding activity of both 3C derivatives was on par with wt protein (Table 3). Because the proteolytic and RNA-binding activities are the only known activities of 3C(D) or its precursors that could have an effect on translation and/or genome replication, these data may suggest more new functions for 3CD. It is well known that poliovirus genome replication can be inhibited by brefeldin A, an inhibitor of ER-to-Golgi trafficking (71–73). Recently, the Ehrenfeld laboratory showed that introduction of 3CD protein into a HeLa cell-free extracts caused stable association of a brefeldin-A-targeted guanine-nucleotide exchange factors with membranes (60–63). Importantly, this activity of 3CD appears to be essential for genome replication, presumably by facilitating formation of the vesicular clusters that are induced by the virus and employed for genome replication (60–63). It is possible that the E24A and E96A/E99A mutants are defective in this novel pre-replication function of 3CD.

### VPg Uridylylation Functions

The final class of mutants encoded 3C proteins that exhibited changes in VPg uridylylation activity that were unrelated to RNA binding activity (Figs. 6 and 7). These mutants were: E24A, E45A, D50A, E71A and E96A/E99A. It was the isolation of this class of mutants that was the primary motivation for this study, identification of a 3C surface that interacts with 3Dpol. Interestingly, 3C-E24A and 3C-D50A exhibited gain-of-function for VPg uridylylation (Fig. 7). As discussed above, E24A, E71A and E96A/E99A mutants also exhibited significant defects to virus multiplication that could not be attributed to VPg uridylylation. Substantial (10 fold) reductions in VPg uridylylation in vitro did not correlate directly with reductions in genome replication (e.g. compare VPg uridylylation to RNA synthesis in Table 3 for the E45A and E96A/E99A mutants). This observation is consistent with our previous study that concluded VPg uridylylation does not limit the rate of PV genome replication in tissue culture and that VPg-pUpU may be produced in vast excess of that needed for PV genome replication (14). Most of the residues of 3C implicated in VPg uridylylation by this study are located on a single convex surface of the 3C dimer (Fig. 9D). However, E96 and D99 are at remote sites in a dynamic region of the protein. These residues clearly use an indirect mechanism, perhaps molecular dynamics, to alter the stability of the $3C_2$-3Dpol complex. Consistent with this surface interacting with 3Dpol, both the E45A and E96A/E99A mutants exhibited a synthetically lethal defect to genome replication when combined with a mutation encoding the 3Dpol-R455A derivative (Fig. 8). This and related derivatives have been shown by us to be inefficiently recruited to and/or retained in the $3C_2$-oriI complex, presumably due to a sub-optimal interaction of 3Dpol with the 3C dimer (data not shown and (14)).

### Structural Model for the $3C_2$-3Dpol Complex

We employed a molecular docking algorithm to obtain candidate models for the $3C_2$-3Dpol complex. We were able to identify only one solution that was consistent with all of our current and previous molecular genetic and biochemical data (Fig. 9) (13,14,41). An important aspect of this model is that 3Dpol should be able to add to a $3C_2$-oriI complex as a hole sufficient to

accommodate single-stranded RNA is visible in the $3C_2$-3Dpol complex (Fig. 9B). Alignments of picornaviral 3C and 3Dpol proteins (74) suggest that interactions between $3C_2$ and 3Dpol predicted by the model (Table 4) are well conserved across the entire virus family. Residues of 3Dpol known to be involved in VPg uridylylation (e.g. 406, 455 and 461) map to the interface (Fig. 9D) (14,41,69). The Kirkegaard laboratory performed charged-to-alanine-scanning mutagenesis of 3Dpol (42). This study was the first to suggest a role for residues 455 and 456 in some aspect of genome replication (42). That study also identified many other residues that were required for genome replication that remain to be characterized. Many of these map on or very near the surface of 3Dpol proposed to interact with $3C_2$ (Fig. 10A). Importantly, some of these mutants rendered virus multiplication temperature sensitive, perhaps representing the first PV mutants that are temperature sensitive for VPg uridylylation. The DeRisi laboratory recently reported unexpected levels of diversity in 3C- and 3Dpol-coding sequence for human rhinoviruses (75). The only other region of the genome with a similar density of diversity is capsid-coding sequence, which is clearly under pressure to escape the humoral immune response. Interestingly, many of the residues in 3Dpol (panel i of Fig. 10B) and 3C (panel ii of Fig. 10B) under purifying selective pressure map on or very near the $3C_2$-3Dpol interface. It is possible that the overlap between pre-replication and VPg uridylylation functions of 3CD reported here is driving the rapid evolution of these regions of the genome. Together, these data add validity to our structural model, moving studies of picornavirus VPg uridylylation into the structural era.

**Acknowledgements**

We thank Professor Coray Colina for helpful discussions regarding construction and evaluation of the structural model for $3C_2$-3Dpol. We thank Hyung Suk Oh for assistance with infectious-center and luciferase assays.

## References

1. Racaniello, VR. Picornaviridae: The viruses and their replication. In: Knipe, DM.; Howley, PM.; Griffin, DE.; Lamb, RA.; Martin, MA.; Roizman, B.; Straus, SE., editors. Fields Virology. 4. Lippincott-Raven Publishers; Philadelphia, PA: 2001.
2. Semler, BL.; Wimmer, E., editors. Molecular Biology of Picornaviruses. ASM Press; Washington, D.C.: 2002.
3. Paul, AV. Possible Unifying Mechanism of Picornavirus Genome Replication. In: Semler, BL.; Wimmer, E., editors. Molecular Biology of Picornaviruses. 1. ASM Press; Washington, D.C: 2002.
4. Paul AV, van Boom JH, Filippov D, Wimmer E. Nature 1998;393(6682):280–284. [PubMed: 9607767]
5. Paul AV, Rieder E, Kim DW, van Boom JH, Wimmer E. J Virol 2000;74(22):10359–10370. [PubMed: 11044080]
6. Rieder E, Paul AV, Kim DW, van Boom JH, Wimmer E. J Virol 2000;74(22):10371–10380. [PubMed: 11044081]
7. Goodfellow I, Chaudhry Y, Richardson A, Meredith J, Almond JW, Barclay W, Evans DJ. J Virol 2000;74(10):4590–4600. [PubMed: 10775595]
8. Morasco BJ, Sharma N, Parilla J, Flanegan JB. J Virol 2003;77(9):5136–5144. [PubMed: 12692216]
9. Murray KE, Barton DJ. J Virol 2003;77(8):4739–4750. [PubMed: 12663781]
10. van Ooij MJ, Vogt DA, Paul A, Castro C, Kuijpers J, van Kuppeveld FJ, Cameron CE, Wimmer E, Andino R, Melchers WJ. J Gen Virol 2006;87(Pt 1):103–113. [PubMed: 16361422]
11. Gerber K, Wimmer E, Paul AV. J Virol 2001;75(22):10979–10990. [PubMed: 11602738]
12. Nayak A, Goodfellow IG, Belsham GJ. J Virol 2005;79(12):7698–7706. [PubMed: 15919922]
13. Pathak HB, Arnold JJ, Wiegand PN, Hargittai MR, Cameron CE. J Biol Chem 2007;282(22):16202–16213. [PubMed: 17392285]
14. Shen M, Wang Q, Yang Y, Pathak HB, Arnold JJ, Castro C, Lemon SM, Cameron CE. J Virol. 2007 Sep 12;Epub ahead of print
15. Harris KS, Reddigari SR, Nicklin MJ, Hammerle T, Wimmer E. J Virol 1992;66(12):7481–7489. [PubMed: 1331532]

16. Marcotte LL, Wass AB, Gohara DW, Pathak HB, Arnold JJ, Filman DJ, Cameron CE, Hogle JM. J Virol. 2007
17. Andino R, Rieckhof GE, Achacoso PL, Baltimore D. Embo J 1993;12(9):3587–3598. [PubMed: 8253083]
18. Bergmann EM, Mosimann SC, Chernaia MM, Malcolm BA, James MN. J Virol 1997;71(3):2436–2448. [PubMed: 9032381]
19. Blair WS, Nguyen JH, Parsley TB, Semler BL. Virology 1996;218(1):1–13. [PubMed: 8615011]
20. Blair WS, Parsley TB, Bogerd HP, Towner JS, Semler BL, Cullen BR. Rna 1998;4(2):215–225. [PubMed: 9570321]
21. Gamarnik AV, Andino R. J Virol 2000;74(5):2219–2226. [PubMed: 10666252]
22. Hammerle T, Molla A, Wimmer E. J Virol 1992;66(10):6028–6034. [PubMed: 1326654]
23. Harris KS, Xiang W, Alexander L, Lane WS, Paul AV, Wimmer E. J Biol Chem 1994;269(43):27004–27014. [PubMed: 7929441]
24. Kusov YY, Gauss-Muller V. Rna 1997;3(3):291–302. [PubMed: 9056766]
25. Leong LE, Walker PA, Porter AG. J Biol Chem 1993;268(34):25735–25739. [PubMed: 8245010]
26. Ohlenschlager O, Wohnert J, Bucci E, Seitz S, Hafner S, Ramachandran R, Zell R, Gorlach M. Structure 2004;12(2):237–248. [PubMed: 14962384]
27. Parsley TB, Towner JS, Blyn LB, Ehrenfeld E, Semler BL. Rna 1997;3(10):1124–1134. [PubMed: 9326487]
28. Peters H, Kusov YY, Meyer S, Benie AJ, Bauml E, Wolff M, Rademacher C, Peters T, Gauss-Muller V. Biochem J 2005;385(Pt 2):363–370. [PubMed: 15361063]
29. Shih SR, Chiang C, Chen TC, Wu CN, Hsu JT, Lee JC, Hwang MJ, Li ML, Chen GW, Ho MS. J Biomed Sci 2004;11(2):239–248. [PubMed: 14966374]
30. Walker PA, Leong LE, Porter AG. J Biol Chem 1995;270(24):14510–14516. [PubMed: 7782313]
31. Xiang W, Harris KS, Alexander L, Wimmer E. J Virol 1995;69(6):3658–3667. [PubMed: 7745714]
32. Yang Y, Rijnbrand R, Watowich S, Lemon SM. J Biol Chem 2004;279(13):12659–12667. [PubMed: 14711816]
33. Yin J, Paul AV, Wimmer E, Rieder E. J Virol 2003;77(9):5152–5166. [PubMed: 12692218]
34. Zell R, Sidigi K, Bucci E, Stelzner A, Gorlach M. Rna 2002;8(2):188–201. [PubMed: 11911365]
35. Amero CD, Arnold JJ, Moustafa IM, Cameron CE, Foster MP. J Virol. 2007submitted
36. Thiviyanathan V, Yang Y, Kaluarachchi K, Rijnbrand R, Gorenstein DG, Lemon SM. Proc Natl Acad Sci U S A 2004;101(34):12688–12693. [PubMed: 15314212]
37. Ferrer-Orta C, Arias A, Agudo R, Perez-Luque R, Escarmis C, Domingo E, Verdaguer N. Embo J 2006;25(4):880–888. [PubMed: 16456546]
38. Pathak, HB. Biochemistry and Molecular Biology. The Pennsylvania State University; University Park: 2006. Toward a unified model for initiation of the first step of picornavirus genome replication.
39. Tellez AB, Crowder S, Spagnolo JF, Thompson AA, Peersen OB, Brutlag DL, Kirkegaard K. J Mol Biol 2006;357(2):665–675. [PubMed: 16427083]
40. Paul AV, Yin J, Mugavero J, Rieder E, Liu Y, Wimmer E. J Biol Chem 2003;278(45):43951–43960. [PubMed: 12937178]
41. Pathak HB, Ghosh SK, Roberts AW, Sharma SD, Yoder JD, Arnold JJ, Gohara DW, Barton DJ, Paul AV, Cameron CE. J Biol Chem 2002;277(35):31551–31562. [PubMed: 12077141]
42. Diamond SE, Kirkegaard K. J Virol 1994;68(2):863–876. [PubMed: 8289389]
43. Dmitrieva TM, Alexeevski AV, Shatskaya GS, Tolskaya EA, Gmyl AP, Khitrina EV, Agol VI. Virology 2007;365(1):79–91. [PubMed: 17467026]
44. Herold J, Andino R. J Virol 2000;74(14):6394–6400. [PubMed: 10864650]
45. Gohara DW, Crotty S, Arnold JJ, Yoder JD, Andino R, Cameron CE. J Biol Chem 2000;275(33):25523–25532. [PubMed: 10827187]
46. Caliguiri LA, Tamm I. Virology 1968;35(3):408–417. [PubMed: 4298649]
47. Noble J, Levintow L. Virology 1970;40(3):634–642. [PubMed: 4314509]
48. Tershak DR. J Virol 1982;41(1):313–318. [PubMed: 6283124]

49. Barton DJ, Morasco BJ, Flanegan JB. Methods Enzymol 1996;275:35–57. [PubMed: 9026649]
50. Lyons T, Murray KE, Roberts AW, Barton DJ. J Virol 2001;75(22):10696–10708. [PubMed: 11602711]
51. Gohara DW, Ha CS, Kumar S, Ghosh B, Arnold JJ, Wisniewski TJ, Cameron CE. Protein Expr Purif 1999;17(1):128–138. [PubMed: 10497078]
52. Jones TA, Zou JY, Cowan SW, Kjeldgaard M. Acta Crystallogr A 1991;47(Pt 2):110–119. [PubMed: 2025413]
53. Phillips JC, Braun R, Wang W, Gumbart J, Tajkhorshid E, Villa E, Chipot C, Skeel RD, Kale L, Schulten K. J Comput Chem 2005;26(16):1781–1802. [PubMed: 16222654]
54. Humphrey W, Dalke A, Schulten K. J Mol Graph 1996;14(1):33–38. 27–38. [PubMed: 8744570]
55. Hansen JL, Long AM, Schultz SC. Structure 1997;5(8):1109–1122. [PubMed: 9309225]
56. Hobson SD, Rosenblum ES, Richards OC, Richmond K, Kirkegaard K, Schultz SC. Embo J 2001;20 (5):1153–1163. [PubMed: 11230138]
57. Lyle JM, Bullitt E, Bienz K, Kirkegaard K. Science 2002;296(5576):2218–2222. [PubMed: 12077417]
58. Pata JD, Schultz SC, Kirkegaard K. Rna 1995;1(5):466–477. [PubMed: 7489508]
59. Mosimann SC, Cherney MM, Sia S, Plotch S, James MN. J Mol Biol 1997;273(5):1032–1047. [PubMed: 9367789]
60. Belov GA, Altan-Bonnet N, Kovtunovych G, Jackson CL, Lippincott-Schwartz J, Ehrenfeld E. J Virol 2007;81(2):558–567. [PubMed: 17079330]
61. Belov GA, Ehrenfeld E. Cell Cycle 2007;6(1):36–38. [PubMed: 17245115]
62. Belov GA, Fogg MH, Ehrenfeld E. J Virol 2005;79(11):7207–7216. [PubMed: 15890959]
63. Belov GA, Habbersett C, Franko D, Ehrenfeld E. J Virol. 2007
64. Franco D, Pathak HB, Cameron CE, Rombaut B, Wimmer E, Paul AV. J Virol 2005;79(10):6358–6367. [PubMed: 15858019]
65. Franco D, Pathak HB, Cameron CE, Rombaut B, Wimmer E, Paul AV. Virol J 2005;2:86. [PubMed: 16300678]
66. Wimmer E, Hellen CU, Cao X. Annu Rev Genet 1993;27:353–436. [PubMed: 8122908]
67. Thompson AA, Peersen OB. Embo J 2004;23(17):3462–3471. [PubMed: 15306852]
68. Tovchigrechko A, Vakser IA. Nucleic Acids Res 2006;34(Web Server issue):W310–314. [PubMed: 16845016]
69. Pathak HB, Cameron CE. 2007unpublished observations
70. Hammerle T, Hellen CU, Wimmer E. J Biol Chem 1991;266(9):5412–5416. [PubMed: 1848550]
71. Cuconati A, Molla A, Wimmer E. J Virol 1998;72(8):6456–6464. [PubMed: 9658088]
72. Doedens J, Maynell LA, Klymkowsky MW, Kirkegaard K. Arch Virol 1994;(Suppl 9):159–172. [PubMed: 8198441]
73. Maynell LA, Kirkegaard K, Klymkowsky MW. J Virol 1992;66(4):1985–1994. [PubMed: 1312615]
74. Palmenberg AC. Picornavirus: Sequence alignments & phylogenetic trees. 1996
75. Kistler AL, Webster DR, Rouskin S, Magrini V, Credle JJ, Schnurr DP, Boushey HA, Mardis ER, Li H, DeRisi JL. Virol J 2007;4:40. [PubMed: 17477878]

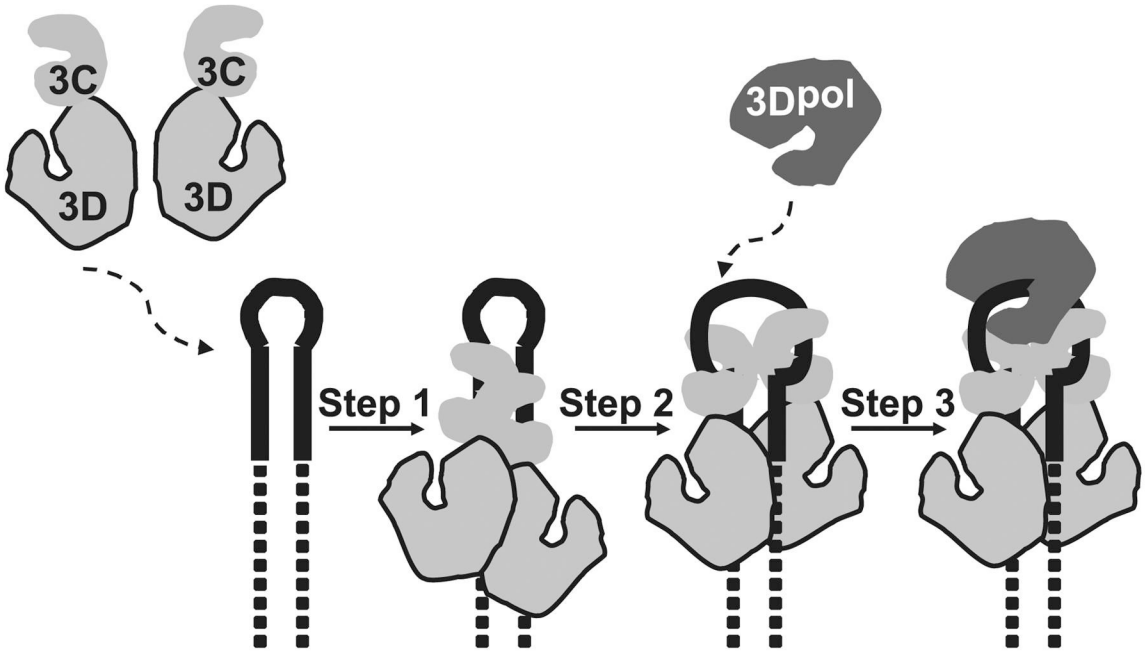


**Figure 1. Assembly and organization of the picornavirus VPg ribonucleoprotein complex**

**Step 1:** Two 3C(D) molecules bind to oriI with the 3C domains contacting the upper stem (solid lines) and the 3D domains contacting the lower stem (dashed lines). **Step 2:** The 3C dimer opens the RNA stem by forming a more stable interaction with single strands forming the stem. **Step 3:** 3Dpol is recruited to and retained in this complex by a physical interaction between the back of the thumb sub-domain of 3Dpol and a surface of one or both 3C subunits of the dimer. Taken from ref. (13).

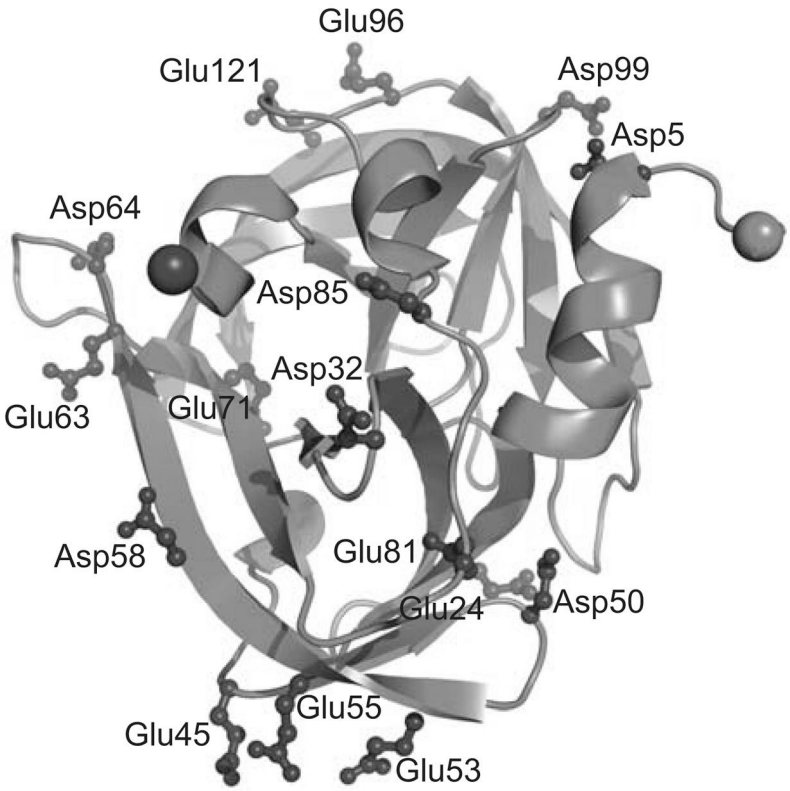


**Figure 2. Solvent accessible acidic amino acid residues of PV 3C**

The structure of PV 3C (1L1N) is shown. The residues targeted for mutational analysis are labeled and shown as ball-and-sticks. The N- and C-termini are displayed as light and dark spheres, respectively.

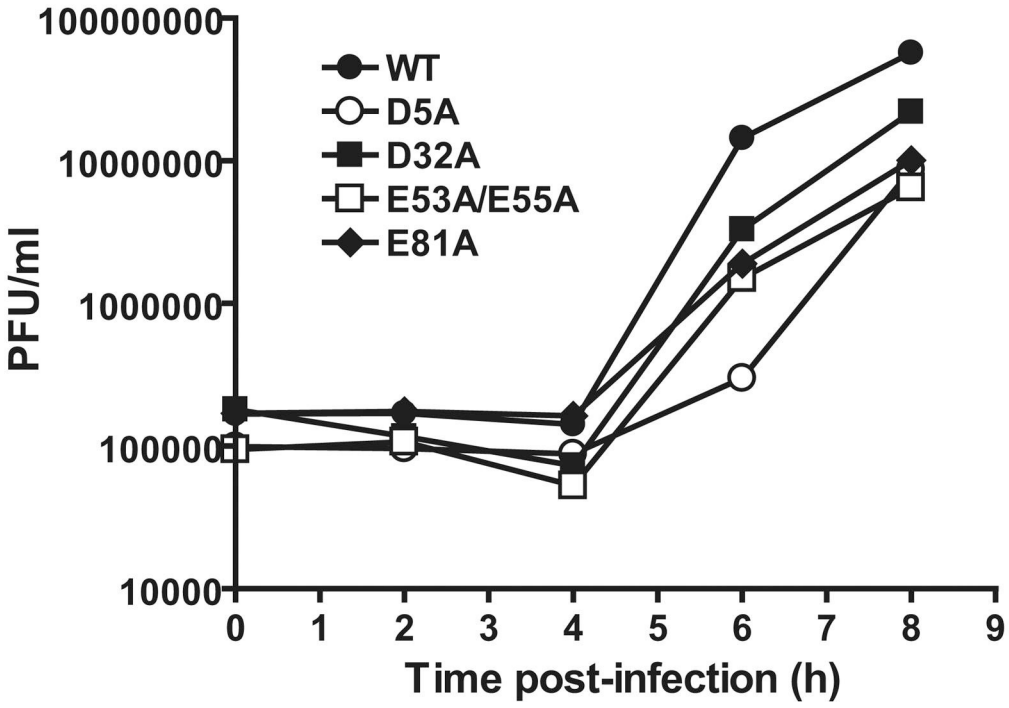


**Figure 3. Kinetics of virus growth for selected PV 3C mutants**

HeLa cells were infected at a multiplicity of infection of 10 with PV encoding WT or the indicated mutant 3C protein. The cells were incubated at 37 °C for 0, 1, 2, 3, 4, 6 and 8 h post-infection. Virus was harvested by 3 repeated freeze-thaw cycles and virus titers were performed by plaque assays on HeLa cells. Viral titer (pfu/mL) was plotted as a function of time post-infection.

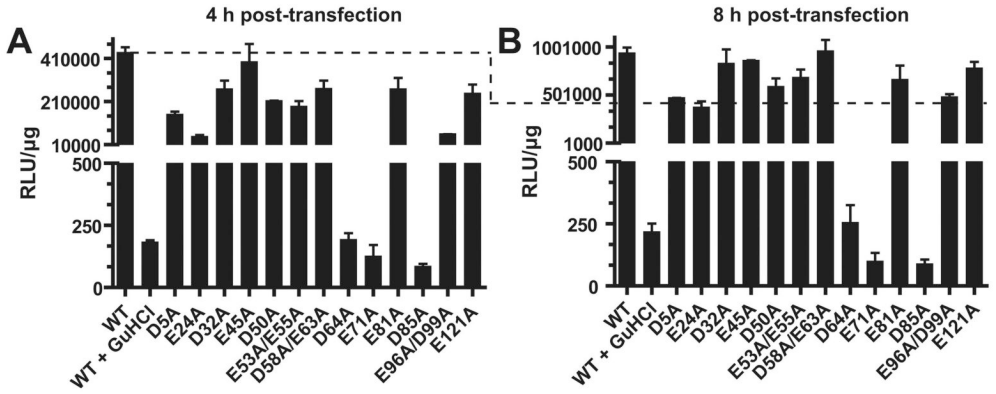


**Figure 4. Kinetics of RNA synthesis using a luciferase-expressing, subgenomic replicon**

HeLa cells were transfected with the indicated replicon RNA (5 µg) and incubated for 4 h (**A**) or 8 h (**B**) post-transfection. Extracts were prepared and analyzed for luciferase activity. Luciferase specific activity is reported in relative light units (RLU) per microgram of total protein in the extract. WT + GuHCl represents a control for translation of input RNA without replication. The dashed line indicates luciferase activity observed for WT at 4 h. The results are the average of two independent transfections of replicon RNA transcribed from two independent clones. Error bars indicate the standard deviation.

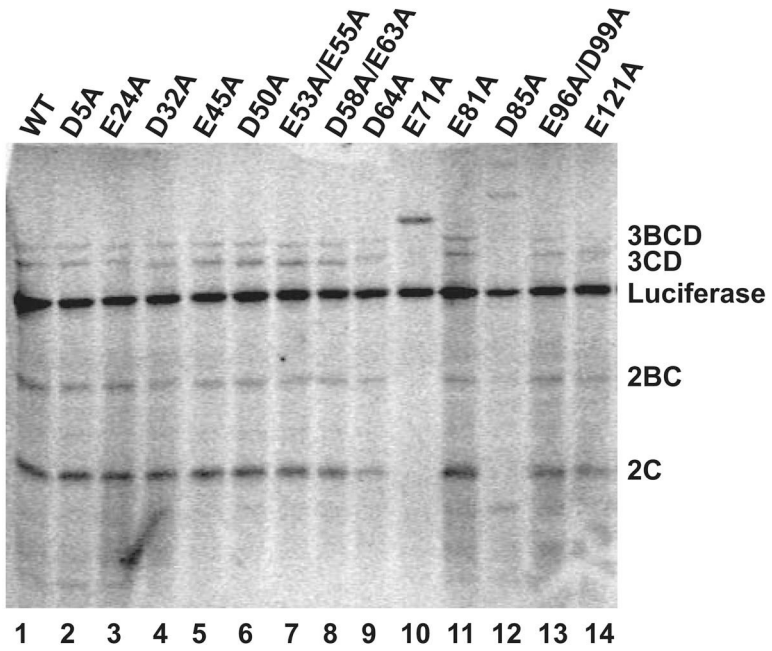


**Figure 5. Proteolytic processing activity of PV 3C mutants**

HeLa extracts containing [$^{35}$S]-methionine were programmed with subgenomic replicon RNAs encoding the indicated 3C protein. After 2 h, samples were mixed with SDS-PAGE sample buffer and resolved by SDS-PAGE on a 12.5% acrylamide gel. Gels were fixed, dried and the radiolabeled proteins were detected by phosphorimaging.

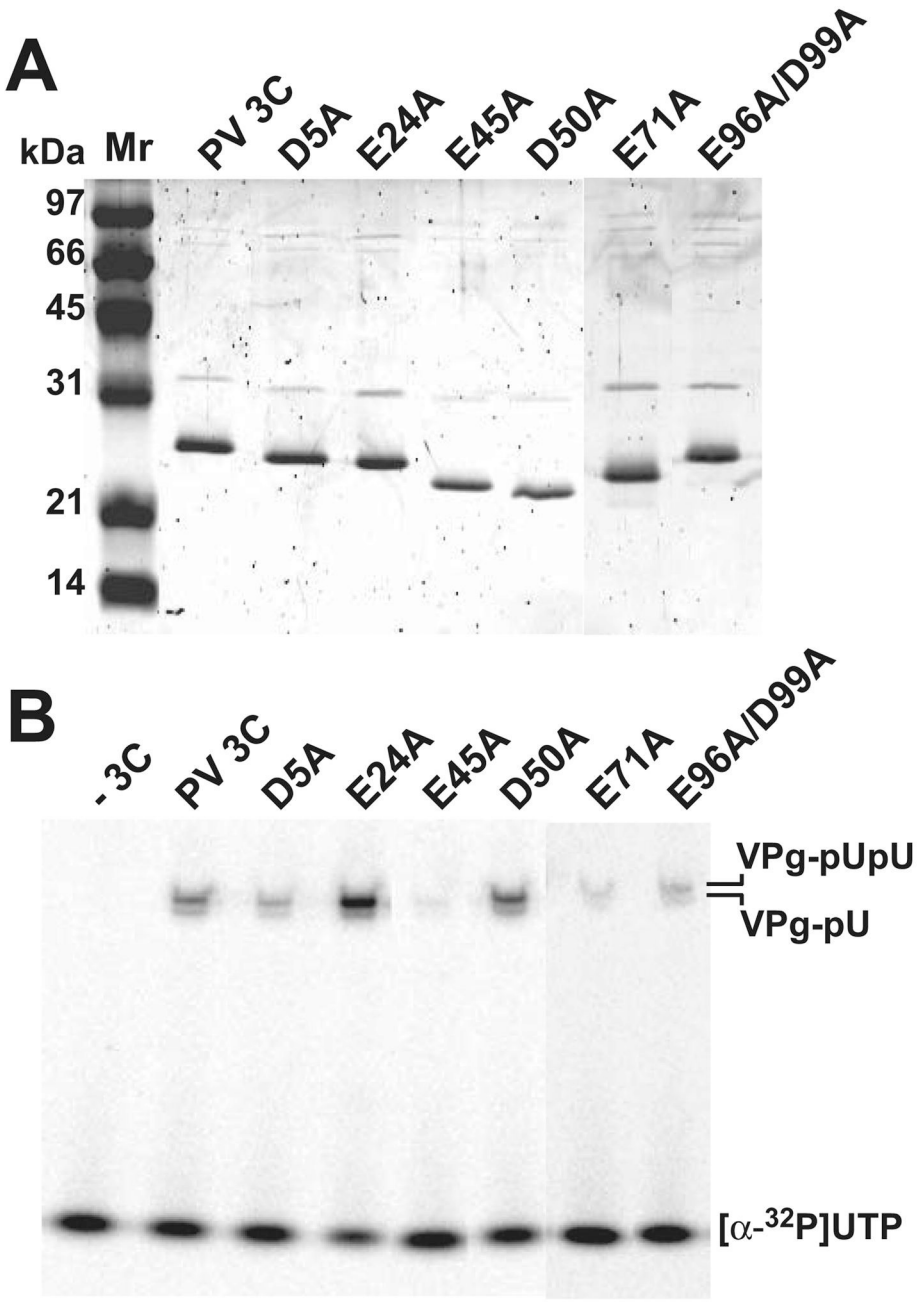


**Figure 6. VPg uridylylation activity of selected PV 3C mutants**

**A.** Sypro stained gel of spin-column-purified proteins (0.1 μg) employed in the VPg uridylylation experiment. The sypro-stained proteins were detected by using a Typhoon-8600 Variable Mode Imager. **B.** VPg uridylylation reactions were performed by using the indicated purified 3C derivative. Uridylylation products were resolved from [α-$^{32}$P]UTP by using a 15% polyacrylamide gel and a Tris-Tricine buffer system. The "-3C" lane indicates a reaction performed in the absence of 3C.

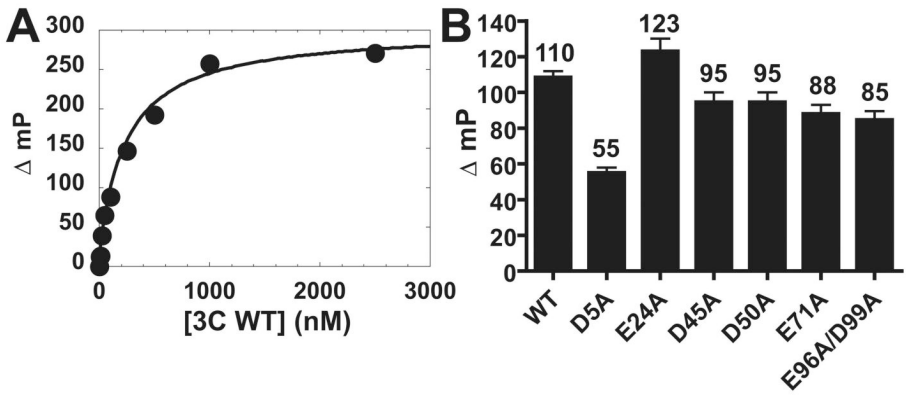


**Figure 7. OriI binding by selected PV 3C derivatives**

**A.** OriI binding by WT 3C. 3′-fluorescein-labeled oriI RNA (29-nt) was titrated with 3C. Binding was measured by monitoring the change in fluorescence polarization (Δ mP). The data were fit to a hyperbola. The $K_d$ value is 260 ± 40 nM. **B.** OriI binding by 3C derivatives. 3C protein (150 nM) was mixed with 3′-fluorescein labeled oriI RNA and the change in polarization (Δ mP) was measured. The results are the average of three independent binding experiments with error bars indicating the standard deviation.

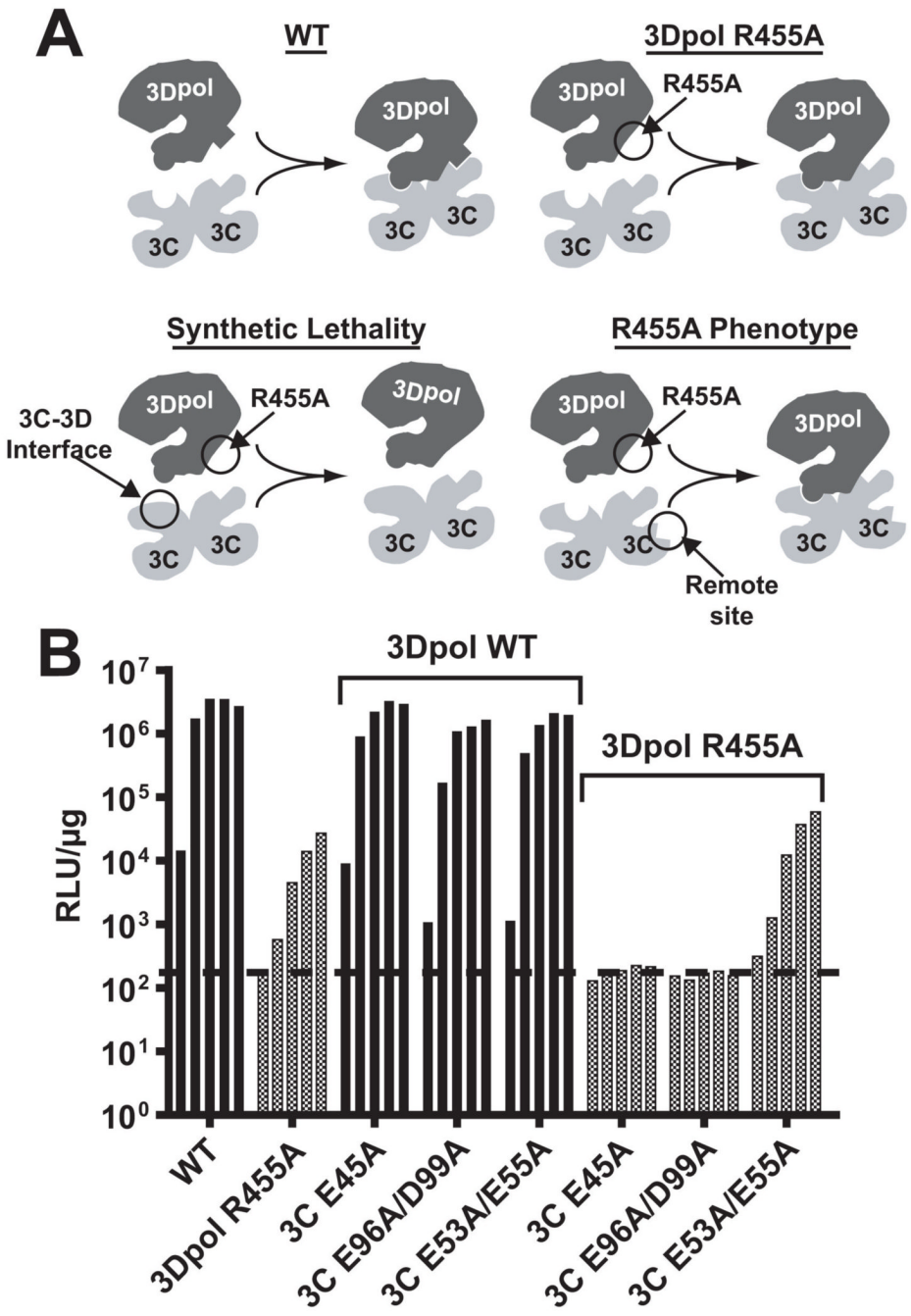


**Figure 8. PV mutants encoding substitutions in 3C residues proposed to interact with 3Dpol exhibit synthetic lethality in a PV background producing 3Dpol R455A**

**A**. Conceptual framework for this experiment. (i) WT $3C_2$ and 3Dpol interact via specific surface residues. (ii) R455A mutation in 3Dpol weakens $3C_2$-3Dpol interaction and reduced replication occurs. (iii) R455A 3Dpol mutation combined with $3C_2$ interaction surface mutation disrupts $3C_2$-3Dpol interaction and prevents replication (synthetic lethality). (iv) R455A 3Dpol mutation combined with $3C_2$ remote site (non-interaction surface) mutation results in $3C_2$-3Dpol interaction and replication as in (ii). **B**. Replication of WT, 3Dpol-R455A or 3C mutations as indicated in either 3Dpol-WT or 3Dpol R455A background. Luciferase activity (RLU/µg) was determined 2, 4, 6, 8 and 10 h post-transfection into HeLa cells. Dashed

line indicates luciferase activity attributable to translation only. The 3C E45A and E96A/D99A mutants exhibit synthetic lethality in the 3Dpol R455A background, further confirming an interaction of these residues with 3Dpol.

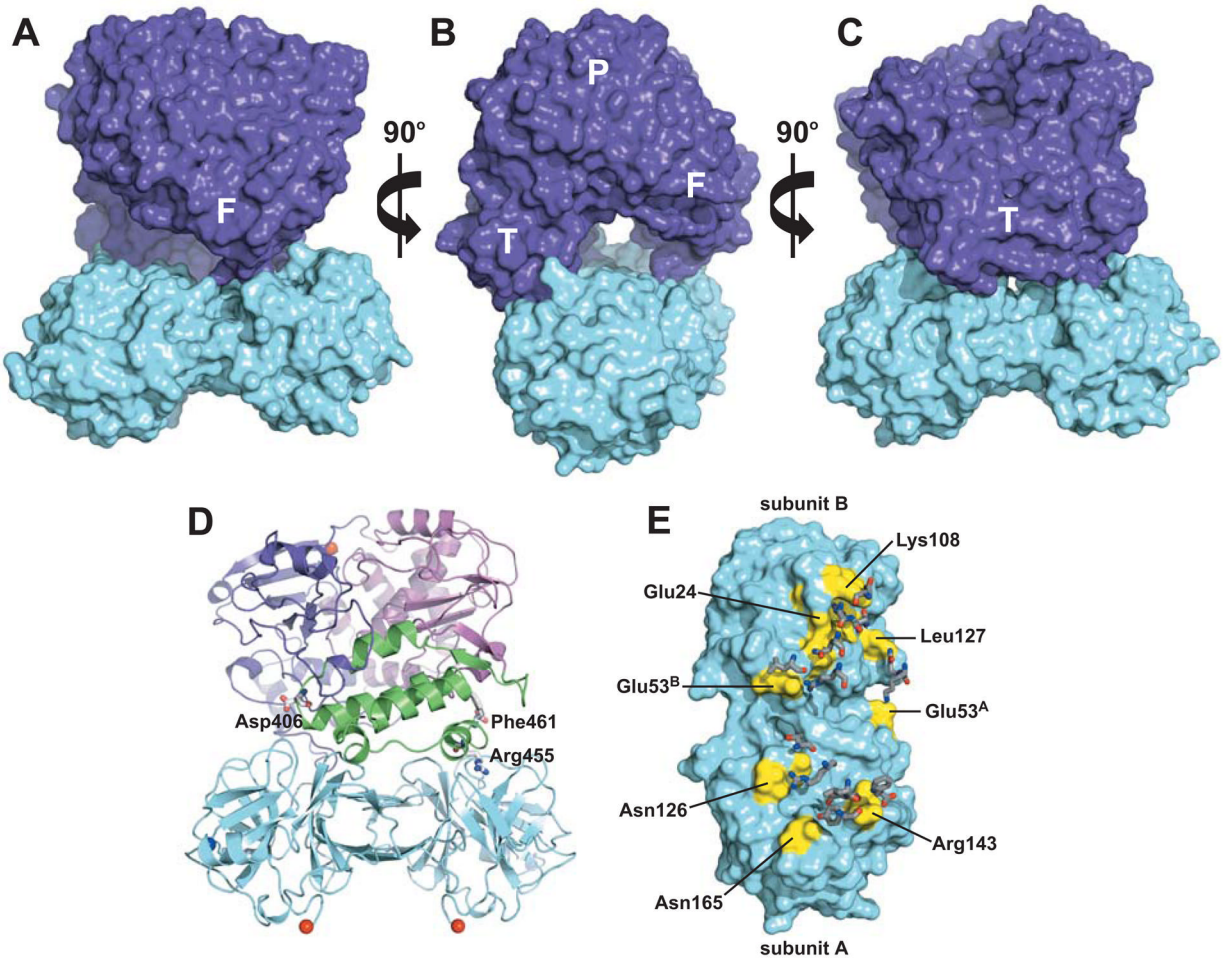


**Figure 9. Model of $3C_2$-3Dpol complex**

**A.** The surfaces of the 3C dimer and 3Dpol are shown in cyan and purple, respectively. The 3Dpol sub-domains are abbreviated as follows: F, fingers; T, thumb; P, palm. **B**. Same as in (A) with 90° rotation around y-axis. **C.** Same as in (A) with 180° rotation around the y-axis **D.** The model of $3C_2$-3Dpol is shown rotated 180° around the Y-axis relative to the view in (A); 3Dpol residues known to be required for VPg uridylylation are shown. These are: Asp406 (14,32), Arg455 (38,41) and Phe461 (69). **E.** Residues of the 3C dimer that contribute to interaction with 3Dpol are shown in yellow. Selected 3C residues are shown for orientation. The complementary residues from 3Dpol are displayed as sticks. These interactions are listed in Table 4.

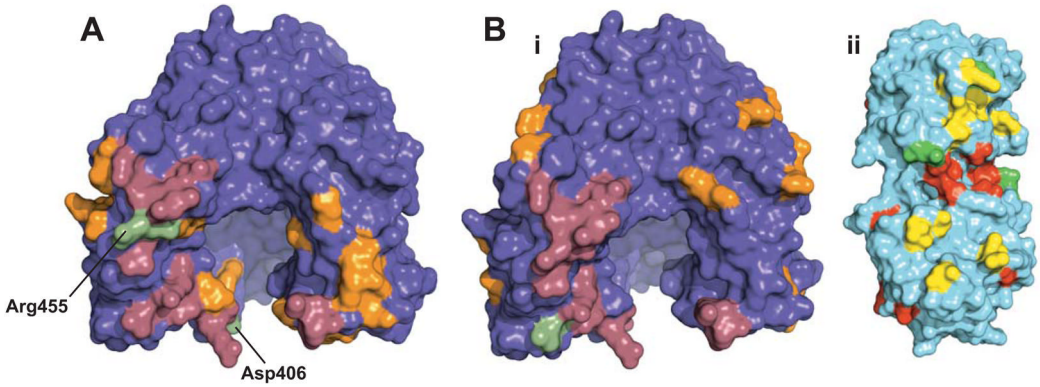


**Figure 10.**

**A. Previously isolated 3Dpol mutants map to the $3C_2$-interaction surface defined in this study.** The 3Dpol surface is colored purple, and regions of 3Dpol involved in $3C_2$-3Dpol interactions are shown in raspberry. 3Dpol mutants constructed in ref. (42) are shown in orange. Those that killed the virus include: Arg128, Lys383, Lys405, Asp406, Asp412, Arg455 and Arg456. Those that caused a temperature-sensitive phenotype include: Glu98, Asp99, Asp105, Glu108, Arg136, Asp137, Glu426, Glu427 and Glu428. Residues that overlap directly with those for which biochemical data exist are underlined above and shown in green on the structure. **B. Diversifying residues on 3C and 3Dpol map to the $3C_2$-3Dpol interface. [i]** The 3Dpol surface is colored purple and regions that interact with the 3C dimer are shown in raspberry. Diversifying residues of 3Dpol identified in ref. (75) are shown in orange including: Met86, Glu93, Thr138, Lys200, Glu254, Gly259, Asp260, Glu369, Pro385, Lys431, and Ala434. Residues identified in both studies are shown in green. **[ii]** The 3C surface is colored in cyan and regions that interact with 3Dpol are shown in yellow. Diversifying residues of 3C identified in ref. (75) are shown in red including: Ser21, Gly44, Glu45, Ser46, Thr68, Tyr109, and Thr120. Residues identified in both studies are shown in green.

**Table 1**

**Oligonucleotides used in this study**

Restriction sites are bold; nucleotide changes are lower case.

| No. | Name | Sequence |
|---|---|---|
| 1 | pMo-SnaBI-F | 5′-TTA TG**T ACG TA**C CAC CAG GAG CTC CAG TGC CCG AG –3′ |
| 2 | pMo-BglII-R | 5′-CGC **AGA TCT** CCA CTT CTT TGC CA –3′ |
| 3 | PV-sil-HpaI-F | 5′-GAA GGG TTG GAT A**GT tAA C**AT CAC CAG CCA GGT TC-3′ |
| 4 | PV-sil-HpaI-R | 5′-GAA CCT GGC TGG TGA T**GT TaA C**TA TCC AAC CCT TC-3′ |
| 5 | pRLuc-SpeI-F | 5′-GCG **ACT AGT** TAT TAT AAC TAG GAA CTA TGA AGA CAC CAC AAC AGT GCT AGC TAC CCT GGC CCT TC |
| 6 | pMo-BglII-F | 5′-GAA GTG G**AG ATC T**TG GAT GCC AAA GCG-3′ |
| 7 | 3D-AflII-R | 5′-AAA GTC TGT **CTT AAG** CCT GGG ATC G-3′ |
| 8 | PV-sil-SacII-F | 5′-CGG TTC ACA CGG GTT TG**C cGC GG**C CCT GAA GCG A -3′ |
| 9 | PV-sil-SacII-R | 5′-TCG CTT CAG GG**C CGC gG**C AAA CCC GTG TGA ACC G-3′ |
| 10 | PV-3C-D5A-F | 5′-CAA GGA CCA GGG TTC gca TAC GCA GTG GCT ATG -3′ |
| 11 | PV-3C-D5A-R | 5′-CAT AGC CAC TGC GTA tgc GAA CCC TGG TCC TTG -3′ |
| 12 | PV-3C-E24A-F | 5′-GTT ACA GCA ACT ACT AGT AAG GGA gcc TTC ACT ATG TTA GGA GTC CAC G -3′ |
| 13 | PV-3C-E24A-R | 5′-CGT GGA CTC CTA ACA TAG TGA Agg cTC CCT TAC TAG TAG TTG CTG TAA C-3′ |
| 14 | PV-3C-D32A-F | 5′-CAC TAT GTT AGG AGT CCA Cgc gAA CGT GGC TAT TTT ACC AA-3′ |
| 15 | PV-3C-D32A-R | 5′-TTG GTA AAA TAG CCA CGT Tcg cGT GGA CTC CTA ACA TAG TG -3′ |
| 16 | PV3C-E45A-F | 5′-ACG CTT CAC CTG GTg ccA GCA TTG TGA TCG ATG GC -3′ |
| 17 | PV3C-E45A-R | 5′-GCC ATC GAT CAC AAT GCT ggc ACC AGG TGA AGC GT -3′ |
| 18 | PV-3C-D50A-F | 5′-ACG CTT CAC CTG GTG AAA GCA TTG TGA TCg cgG GCA AAG AAG TGG AG -3′ |
| 19 | PV-3C-D50A-R | 5′-CTC CAC TTC TTT GCC cgc GAT CAC AAT GCT TTC A -3′ |
| 20 | PV-3C-E53/E55A-F | 5′-GTG ATC GAT GGC AAA gecko GTG gecko ATC TTG GAT GCC A -3′ |
| 21 | PV-3C-E53/E55A-R | 5′-TGG CAT CCA AGA Tgg cCA Cgg cTT TGC CAT CGA TCA C -3′ |
| 22 | PV-3C-D58/E63A-F | 5′-GAA GTG GAG ATC TTG gcg GCC AAA GCG CTC gecko GAT CAA GCA GGA ACC AAT C-3′ |
| 23 | PV-3C-D58/E63A-R | 5′-GAT TGG TTC CTG CTT GAT Cgg cGA GCG CTT TGG Ccg cCA AGA TCT CCA CTT C -3′ |
| 24 | PV-3C-D64A-F | 5′-GCC AAA GCG CTC GAA gca CAA GCA GGA ACC AAT CT -3′ |
| 25 | PV-3C-D64A-R | 5′-AGA TTG GTT CCT GCT TGt gcT TCG AGC GCT TTG GC -3′ |
| 26 | PV-3C-E71A-F | 5′-GCA GGA ACC AAT CTT gecko ATC ACT ATA ATC ACT C -3′ |
| 27 | PV-3C-E71A-R | 5′-GAG TGA TTA TAG TGA Tgg cAA GAT TGG TTC CTG C -3′ |
| 28 | PV-3C-E81A-F | 5′-CAC TAT AAT CAC TCT AAA GAG AAA Tgc tAA GTT CAG AGA CAT TAG ACC ACA -3′ |
| 29 | PV-3C-E81A-R | 5′-TGT GGT CTA ATG TCT CTG AAC TTa gcA TTT CTC TTT AGA GTG ATT ATA GTG -3′ |
| 30 | PV-3C-D85A-F | 5′-GAG AAA TGA AAA GTT CAG Agc gAT TAG ACC ACA TAT AC -3′ |
| 31 | PV-3C-D85A-R | 5′-GTA TAT GTG GTC TAA Tcg cTC TGA ACT TTT CAT TTC TC -3′ |
| 32 | PV-3C-E96/D99A-F | 5′-ACC TAC TCA AAT CAC Tgc cAC AAA Tgc gGG AGT CTT GAT CGT G -3′ |
| 33 | PV-3C-E96/D99A-R | 5′-CAC GAT CAA GAC TCC cgc ATT TGT ggc AGT GAT TTG AGT AGG T -3′ |
| 34 | PV-3C-E121A-F | 5′-GTC GGT GCT GTG ACT gecko CAG GGA TAT CTA AAT CTC -3′ |
| 35 | PV-3C-E121A-R | 5′-GAG ATT TAG ATA TCC CTG ggc AGT CAC AGC ACC GAC -3′ |
| 36 | GSSG-6H-EcoRI-R | 5′-CCG GAA TTC CCA TGG CTA TTA ATG GTG GTG ATG GTG GTG ACC AGA GGA TCC –3′ |
| 37 | pMo-R455A-F | 5′-TAC TCA ACA TTG TAC gct CGT TGG CTT GAC TCA TTT TAG-3′ |
| 38 | pMo-R455A-R | 5′-CTA AAA TGA GTC AAG CCA ACG agc GTA CAA TGT TGA GTA-3′ |
| 39 | pMo-EcoRI-F | 5′-GAA TTA AAT CAT CGA T**GA ATT C**GG GCC C-3′ |
| 40 | pUC18-PHBKBSE-Top | 5′-GGT TAA CGG ATC C**GG TAC C**AG ATC T**CC GCG G**G-3′ |
| 41 | pUC18-PHBKBSE-Bot | 5′-AAT TC**C CGC GG**A GAT CT**G GTA CC**G GAT CCG TTA ACC TGC A-3′ |

## Table 2

**Poliovirus 3C residues targeted for mutational analysis**

| PV 3C mutant | Targeted residue | Proposed function | Type of substitution |
|---|---|---|---|
| 1 | Asp 5 | RNA recognition | single |
| 2 | Glu 24 | none | single |
| 3 | Asp 32 | RNA recognition | single |
| 4 | Glu 45 | Intermolecular contacts | single |
| 5 | Asp 50 | none | single |
| 6 | Glu 53 / Glu 55 | None / intermolecular contacts | double |
| 7 | Asp 58 / Glu 63 | Intermolecular contacts | double |
| 8 | Asp 64 | none | single |
| 9 | Glu 71 | Proteolytic active site | single |
| 10 | Glu 81 | RNA recognition | single |
| 11 | Asp 85 | RNA recognition | single |
| 12 | Glu 96 / Asp 99 | none | double |
| 13 | Glu 121 | none | single |

**Table 3**

**Summary of phenotypes observed for surface-acidic-to-alanine mutants of 3C**

All values are presented as a fraction of wt where indicated.

| Mutation | Specific Infectivity[a] | Virus Growth (6h)[b] | RNA Synthesis (4h)[c] | Processing | 3C Protein Solubility | VPg-pU(pU) Uridylylation[d] | oriI Binding[e] |
|---|---|---|---|---|---|---|---|
| D5A | 1 | 0.02 | 0.3 | + | + | 0.4 | 0.5 |
| E24A | 0.01 | nd[f] | 0.1 | + | + | 2.0 | 1.1 |
| D32A | 1 | 0.2 | 0.6 | + | + | 1.2 | 1.1 |
| E45A | 1 | 0.6 | 0.9 | + | + | 0.1 | 0.9 |
| D50A | 1 | 0.8 | 0.5 | + | + | 1.4 | 0.9 |
| E53A/E55A | 1 | 0.1 | 0.4 | + | + | 1.0 | 1.0 |
| D58A/E63A | 1 | 0.1 | 0.6 | + | + | 0.8 | 0.7 |
| D64A | 0 | nd | 0 | + | + | 0.9 | 0.7 |
| E71A | 0 | nd | 0 | − | + | 0.1 | 0.8 |
| E81A | 1 | 0.1 | 0.6 | + | + | 0.9 | 1.0 |
| D85A | 0 | nd | 0 | − | − | nd | nd |
| E96A/D99A | 0.01 | nd | 0.1 | + | + | 0.3 | 0.8 |
| E121A | 1 | 0.6 | 0.6 | + | + | 0.7 | 0.8 |

[a] wt showed a specific infectivity of $6 \times 10^4$ pfu/μg RNA

[b] wt showed a titer of $1.5 \times 10^7$ pfu/mL at 6 h post-infection

[c] wt showed $4 \times 10^5$ RLU/μg at 4 h post-transfection

[d] wt showed 2 μM VPg-pU(pU) uridylylation in 30 min

[e] wt showed a ΔmP value of 110 at 150 nM

[f] not determined

**Table 4**

**Side chain interactions in the $3C_2$ – 3Dpol complex**

| $3C^A$ – 3Dpol[a] | $3C^B$ – 3Dpol | 3C – 3C[b] |
|---|---|---|
| Glu53 – Lys133 | Leu127 – Gln134 | Lys22 – Glu45 |
| Asn165 – Tyr384 | Lys108 – Asp406 | Ser42 – Glu45 |
| Gly128 – Thr452 | Glu24/Phe25/Thr106 – Arg408 Lys108/Tyr109/Gly145 | Asp58 – Lys60 |
| Asn126 – Arg455 | Lys108 – Asn409 | Ile56 – Ala61 |
| Arg143 – Leu458 Phe461 | Thr19 – Gln411 | Glu63 – Lys78 |
| Ala144 – Asp459 | Glu53 – Arg415 | $Glu55^A$ – $Asn69^B$ |
| | Glu53 – Leu446 | $Arg130^A$ – $Glu55^B$ |

[a] The two subunits of the 3C-dimer are designated A and B.

[b] Most of the interactions between the two monomers in the 3C-dimer are symmetrical. Asymmetrical interactions are designated with the chain labels A/B.